

Anisotropic intrinsic lattice thermal conductivity of phosphorene from first principles

Guangzhao Qin,¹ Qing-Bo Yan,^{1,*} Zhenzhen Qin,² Sheng-Ying Yue,³ Ming Hu,^{4,5,†} and Gang Su^{3,‡}

¹College of Materials Science and Opto-Electronic Technology,
University of Chinese Academy of Sciences, Beijing 100049, China

²College of Electronic Information and Optical Engineering, Nankai University, Tianjin 300071, China

³School of Physics, University of Chinese Academy of Sciences, Beijing 100049, China

⁴Institute of Mineral Engineering, Division of Materials Science and Engineering,
Faculty of Georesources and Materials Engineering,
RWTH Aachen University, Aachen 52064, Germany

⁵Aachen Institute for Advanced Study in Computational Engineering Science (AICES),
RWTH Aachen University, Aachen 52062, Germany

(Dated: February 6, 2015)

Phosphorene, the single layer counterpart of black phosphorus, is a novel two-dimensional semiconductor with high carrier mobility and a large fundamental direct band gap, which has attracted tremendous interest recently. Its potential applications in nano-electronics and thermoelectrics call for a fundamental study of the phonon transport. Here, we calculate the intrinsic lattice thermal conductivity of phosphorene by solving the phonon Boltzmann transport equation (BTE) based on first-principles calculations. The thermal conductivity of phosphorene at 300 K is $30.15 \text{ Wm}^{-1}\text{K}^{-1}$ (zigzag) and $13.65 \text{ Wm}^{-1}\text{K}^{-1}$ (armchair), showing an obvious anisotropy along different directions. The calculated thermal conductivity fits perfectly to the inverse relation with temperature when the temperature is higher than Debye temperature ($\Theta_D = 278.66 \text{ K}$). In comparison to graphene, the minor contribution around 5% of the ZA mode is responsible for the low thermal conductivity of phosphorene. In addition, the representative mean free path (MFP), a critical size for phonon transport, is also obtained.

Black phosphorus (BP) has a puckered layered honeycomb structure with layers held together by *van der Waals* forces, which is similar to graphite.¹⁻³ Few-layer BP has been successfully mechanically exfoliated^{4,5} and attracted tremendous interest recently.⁴⁻¹⁸ Phosphorene, the single layer counterpart of BP, is a novel anisotropic two-dimensional (2D) semiconductor with high carrier mobility⁴⁻⁶ and a large fundamental direct band gap $\sim 1.5 \text{ eV}$,¹⁰ promising its potential applications in nano-electronics besides the already known 2D semiconductors such as graphene, germanane, silicene and transition metal dichalcogenides (TMDCs).³ There have already been a lot of theoretical and experimental works exploring the possible applications of phosphorene as nano-electronic devices, such as field-effect transistors and photo-transistors.⁴⁻⁹ In addition to extensive studies on its electrical properties, there are also a lot of theoretical explorations on its potential applications in thermoelectrics.¹³⁻¹⁵ Phosphorene is found possessing a high ZT value, implying it a potential good thermoelectric material.^{14,15}

All these electrical and thermoelectrical applications of phosphorene are closely related to its thermal properties. However, the thermal conductivity of bulk BP was only roughly measured about fifty years ago¹⁹ and the thermal conductivity of phosphorene was just simply estimated theoretically recently¹⁵. Considering the potential valuable applications of phosphorene as nano-electronic and thermoelectric devices, it is necessary to fundamentally study the thermal conductivity and phonon transport in this new 2D material from first principles.

In this paper, we calculate the intrinsic lattice thermal

conductivity of phosphorene by solving the phonon Boltzmann transport equation (BTE) based on first-principles calculations. The thermal conductivity of phosphorene is found anisotropic, and the calculated thermal conductivity fits perfectly to the inverse relation with temperature when the temperature is higher than Debye temperature. Furthermore, we extract the contribution and the relaxation time of each phonon branch to investigate the underlying mechanism behind the low thermal conductivity of phosphorene compared to graphene. At last, we get the representative mean free path (MFP) of phosphorene that is important for the study of size effect and nano-engineering.

All first-principles calculations are performed based on the density functional theory (DFT) as implemented in the Vienna *ab-initio* simulation package (VASP)²⁰. The Perdew-Burke-Ernzerhof (PBE)²¹ of generalized gradient approximation (GGA) is chosen as the exchange-correlation functional. The kinetic energy cutoff of wave functions is set as 700 eV, and a Monkhorst-Pack²² k -mesh of $10 \times 8 \times 1$ is used to sample the Brillouin Zone (BZ), with the energy convergence threshold set as 10^{-8} eV . A large vacuum spacing of at least 15 Å is used to hinder interactions between periodic layers arising from the employed periodic boundary condition. All geometries are fully optimized until the maximal Hellmann-Feynman force is no larger than $10^{-4} \text{ eV}/\text{Å}$.

As shown in Fig. 1, the optimized structure of phosphorene possesses a hinge-like structure along the armchair direction, which is distinctly different from the flat graphene and buckled silicene^{13,23-26}. The obtained lattice constants (zigzag: 3.32 Å, armchair: 4.58 Å) are in

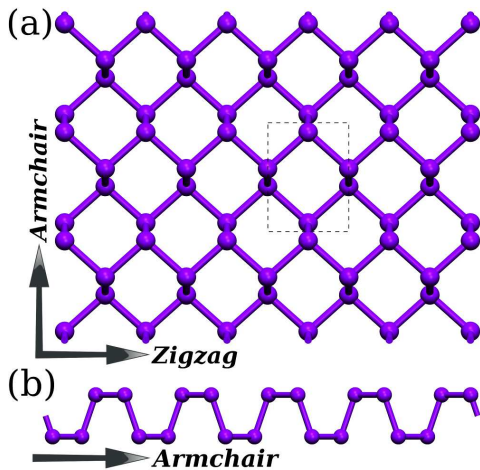


FIG. 1. (Color online) (a) Top view and (b) side view of the monolayer phosphorene. The unit cell is marked with dashed line. The zigzag and armchair directions are indicated with arrows.

good agreement with previous studies^{2,27}. In one unit cell, there are two atoms per layer and four atoms in total, which means 3 acoustic and 9 optical phonon branches.

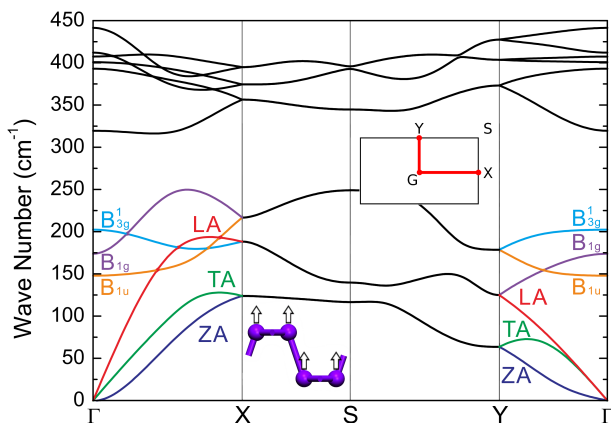


FIG. 2. (Color online) Phonon dispersion along the path passing through the main high-symmetry k -points in BZ of phosphorene. The acoustic phonon branches (ZA, TA and LA) and three optical phonon branches (B_{1u} , B_{1g} and B_{3g}^1) are indicated with different colors. The BZ with high symmetry k -points indicated and the vibrational direction of the ZA mode are shown in the insets.

In the calculation of phonon dispersion, the $5 \times 5 \times 1$ supercell containing 100 atoms is constructed to ensure the convergence. The Monkhorst-Pack k -mesh of $2 \times 2 \times 1$ is used here to sample the BZ. The harmonic second order interatomic force constants (IFCs) are obtained within the linear response framework by employing the density functional perturbation theory (DFPT) as implemented in the `VASP` code²⁰. Then we could get the phonon dispersion of phosphorene using the `PHONOPY` package²⁸ based on the harmonic second order IFCs. The obtained

phonon dispersion, as shown in Fig. 2, is in consistent with other works^{15,16}.

Similar to graphene and silicene^{23–26}, phosphorene also has a quadratic flexural phonon branch (z -direction acoustic mode, ZA) near the Γ point, which is a typical feature of 2D materials²⁴. The vibrational direction of the ZA mode is exactly perpendicular to the plane, i.e. along the z direction, which is similar to graphene but different from silicene whose flexural phonon mode is not purely out-of-plane vibration^{25,26}. Based on the slopes of the longitudinal acoustic (LA) branch near Γ point, we could get the group velocities along Γ -X (zigzag) and Γ -Y (armchair) as 7.83 km/s and 4.01 km/s, respectively, which are in good agreement with previous results¹⁶. With the highest frequency of normal mode vibration (Debye frequency) $\nu_m = 5.81$ THz, the Debye temperature (Θ_D) could be calculated: $\Theta_D = h\nu_m/k_B = 278.66$ K, where h is the Planck's constant and k_B is the Boltzmann constant.

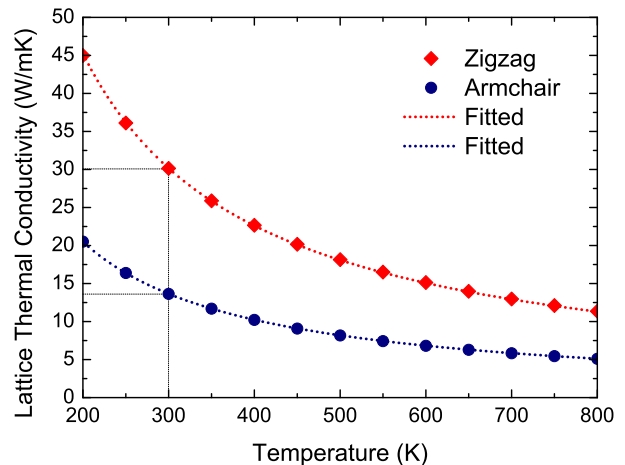


FIG. 3. (Color online) Calculated lattice thermal conductivity (κ) of phosphorene along zigzag (red diamond) and armchair (blue circle) directions as a function of temperature ranging from 200 K to 800 K. The thermal conductivity fitted by the inverse relation with temperature ($\kappa \sim 1/T$) is plotted with dot lines.

For the calculation of lattice thermal conductivity, anharmonic third order IFCs are also necessary besides the harmonic second order IFCs obtained above. The same $5 \times 5 \times 1$ supercell and $2 \times 2 \times 1$ Monkhorst-Pack k -mesh are used to get the anharmonic third order IFCs, and interactions are taken into account up to the fourth nearest neighbors^{29,30}. We additionally obtain the dielectric tensor and Born effective charges based on DFPT for taking into account long-range electrostatic interactions. As a thickness is necessary for the calculation of thermal conductivity for 2D materials, we choose the half of the length of bulk lattice constant along z direction as the thickness of phosphorene, which is 5.36 Å.^{13,31} Only considering the phonon-phonon scattering processes, the intrinsic lattice thermal conductivity could be obtained by solving the phonon BTE as implemented in the `SHENGBTE`

code³². It yields predictive parameter free estimate of thermal conductivity using only basic information of the chemical structure. Detailed information on the workflow could be found in the Supplemental Material.

The intrinsic lattice thermal conductivity (κ) of phosphorene, as shown in Fig. 3, is obviously anisotropic that the thermal conductivity along the zigzag direction is generally twice the thermal conductivity along the armchair direction, which coincides with the previous expectation¹⁵. The anisotropy lies in the asymmetry of group velocities along the Γ -X (zigzag) and Γ -Y (armchair) directions, which may be due to the anisotropic hinge-like structure of phosphorene^{11,13}. Similar anisotropy of thermal conductivity is also found in SnSe, which possesses almost the same hinge-like structure as phosphorene.³³

The thermal conductivity of phosphorene at 300 K is $30.15 \text{ Wm}^{-1}\text{K}^{-1}$ (zigzag) and $13.65 \text{ Wm}^{-1}\text{K}^{-1}$ (armchair). Note that the calculated thermal conductivity along the armchair direction is close to the reported experimental value ($12.1 \text{ Wm}^{-1}\text{K}^{-1}$, with no direction information) of bulk BP¹⁹ while being a little larger, which may be due to the effect of interlayer interactions. The effect of long-range electrostatic interactions introduced from dielectric tensor and Born effective charges is also examined. It is found that the lack of long-range electrostatic interactions would only make the calculated thermal conductivity around 4% smaller. Furthermore, we fit the calculated thermal conductivity along zigzag and armchair directions, respectively, and find that they both satisfy an inverse relation with temperature, i.e. $\kappa \sim 1/T$. The fitted thermal conductivity is also plotted with dot lines in Fig. 3. It is obvious that the fitted thermal conductivity coincides perfectly with the calculated thermal conductivity. The inverse relation of thermal conductivity with temperature that also lies in other materials such as PbSe and $\text{Mg}_2(\text{Si},\text{Sn})$ ^{34,35} has been often observed when the temperature is higher than Debye temperature (Θ_D), which could be explained by the phonon scattering mechanism in pure semiconductors³⁶.

The thermal conductivity of phosphorene is on the same order of magnitude as that of silicene ($5 - 65 \text{ Wm}^{-1}\text{K}^{-1}$)^{25,26,37,38}, while at least two orders of magnitude lower than that of graphene ($3000 - 5000 \text{ Wm}^{-1}\text{K}^{-1}$)^{23,31}. In order to understand the underlying mechanism, we examine the contributions of different phonon branches to the thermal conductivity of phosphorene in both zigzag and armchair directions, as shown in Fig. 4. The contribution of the ZA mode is around 5% at room temperature, which is close to that of silicene (7.5%) but much smaller than that of graphene (75%)^{31,38}. Hence, the reason for the low thermal conductivity of phosphorene might be the same as silicene that is assumed to be due to a small contribution of the ZA mode. Comparing with graphene and silicene, the symmetry-based phonon-phonon scattering selection rule²³ is broke by the puckered hinge-like structure of phosphorene, resulting in a large scattering rate

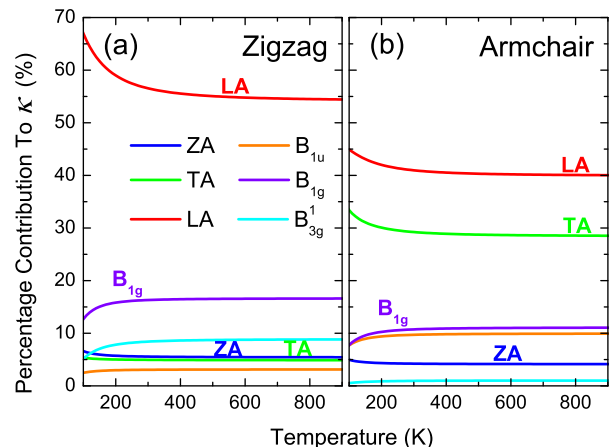


FIG. 4. (Color online) The percentage contribution of each phonon branch to thermal conductivity along (a) zigzag and (b) armchair directions as a function of temperature. Those optical phonon branches contributing less than 1% are not shown.

of the out-of-plane ZA mode, which thus leads to its small contribution to the thermal conductivity. Note that when temperature increases, the contributions of optical phonon branches increase while the contributions of acoustic phonon branches decrease, which might be due to the fact that a high temperature can excite high frequency optical phonon modes that represent the collective opposite vibrations of atoms.

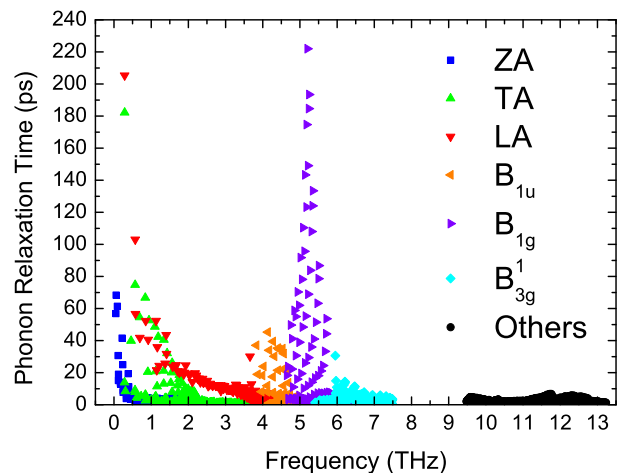


FIG. 5. (Color online) Phonon relaxation time of each phonon branch as a function of frequency.

To gain more information on the contributions of different phonon branches to the thermal conductivity, we extract the relaxation time of each phonon branch as a function of frequency, as shown in Fig. 5. The relaxation time of ZA mode is shorter than that of LA mode and TA mode, which is due to the large scattering rate of ZA mode as discussed above. Thus the ZA mode contributes little to the thermal conductivity, leading to the

low thermal conductivity of phosphorene compared to graphene. It can also be seen that the relaxation time of LA mode is the longest among the three acoustic phonon branches, especially for phonon frequency between 2 and 4 THz. Together with its highest group velocity, it is understandable that the LA mode contributes the most to the thermal conductivity as shown in Fig. 4. Note that the contribution of TA mode is rather large along the armchair direction as shown in Fig. 4(b), which is due to almost the same group velocity of TA mode as LA mode along the Γ -Y (armchair) direction as shown in Fig. 2. Considering the very long relaxation time of the optical phonon branch B_{1g} , the B_{1g} mode contributes much more than other optical phonon branches to the thermal conductivity.

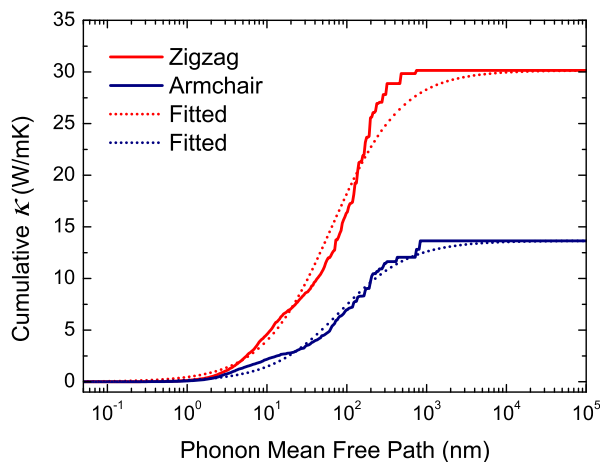


FIG. 6. (Color online) Cumulative lattice thermal conductivity of phosphorene along zigzag (red) and armchair (blue) directions as a function of the phonon MFP at 300 K. The curves fitted by the function presented in text are plotted with dot lines.

The cumulative thermal conductivity (κ) with respect to the phonon MFP at 300 K for both zigzag and armchair directions are plotted in Fig. 6. We fit the data to a single parametric function³²

$$\kappa(l \leq l_{max}) = \frac{\kappa_0}{1 + l_0/l_{max}},$$

where κ_0 and l_{max} are the ultimate cumulated thermal conductivity and the maximal MFP concerned, respectively, and l_0 is the parameter to be evaluated. The fitted curves, as plotted with dot lines in Fig. 6, reproduce the calculated data quite well and yield the parameter l_0 as 66 nm and 83 nm for zigzag and armchair directions, respectively, which could be interpreted as the representative MFP of phosphorene. The representative MFP is helpful for the study of the size effect on the ballistic or diffusive phonon transport. A related quantity is the ratio of thermal conductivity to the thermal conductivity per unit of MFP in the small grain limit, which is an estimate of the characteristic size below which the nanostructuring induced phonon scattering dominates over the anharmonic phonon-phonon scattering. This is critical to thermal design with nanostructuring in that the thermal conductivity could be modulated effectively by nanostructuring when the nanostructure size below the characteristic size. The obtained values for phosphorene are 17 nm (zigzag) and 15 nm (armchair).

In summary, we have calculated the intrinsic lattice thermal conductivity of phosphorene from first principles. The thermal conductivity of phosphorene at 300 K is found to be $30.15 \text{ Wm}^{-1}\text{K}^{-1}$ (zigzag) and $13.65 \text{ Wm}^{-1}\text{K}^{-1}$ (armchair), which is anisotropic along different directions. The calculated thermal conductivity fits perfectly to the inverse relation with temperature when the temperature is higher than Debye temperature ($\Theta_D = 278.66 \text{ K}$). Comparing with graphene, the minor contribution around 5% of the ZA mode is responsible for the low thermal conductivity of phosphorene, which might be due to the fact that the symmetry-based phonon-phonon scattering selection rule is broke by the puckered hinge-like structure of phosphorene. In addition, the representative MFP, a critical size for phonon transport, is also obtained along zigzag and armchair directions.

The authors would like to thank Yingying Li at ZJU, Chao-Sheng Lian at IOP of CAS, Hui-Juan Cui and Prof. Qing-Rong Zheng at UCAS for helpful discussions. This work is supported in part by the NSFC (Grant No. 11004239), the MOST (Grant No. 2012CB932901 and No. 2013CB933401) of China, and the fund from CAS. All calculations are performed on Nebulae (DAWN6000) in National Supercomputing Center in Shenzhen and MagicCube (DAWN5000A) in Shanghai Supercomputer Center, China.

* yan@ucas.ac.cn

† hum@ghi.rwth-aachen.de

‡ gsu@ucas.ac.cn; http://tcmp2.ucas.ac.cn/

¹ A. S. Rodin, A. Carvalho, and H. Castro Neto, A., Phys. Rev. Lett. **112**, 176801 (2014).

² J. Qiao, X. Kong, Z.-X. Hu, F. Yang, and W. Ji, Nat. Commun. **5**, 4475 (2014).

³ H. O. H. Churchill and P. Jarillo-Herrero, Nature Nan-

otech. **9**, 330 (2014).

⁴ H. Liu, A. T. Neal, Z. Zhu, Z. Luo, X. Xu, D. Tomnek, and P. D. Ye, ACS Nano **8**, 4033 (2014).

⁵ L. Li, Y. Yu, G. J. Ye, Q. Ge, X. Ou, H. Wu, D. Feng, X. H. Chen, and Y. Zhang, Nature Nanotech. **9**, 372 (2014).

⁶ F. Xia, H. Wang, and Y. Jia, Nat. Commun. **5**, 4458 (2014).

⁷ T. Low, M. Engel, M. Steiner, and P. Avouris, Phys. Rev.

- B **90**, 081408 (2014).
- ⁸ T. Hong, B. Chamlagain, W. Lin, H.-J. Chuang, M. Pan, Z. Zhou, and Y.-Q. Xu, *Nanoscale* **6**, 8978 (2014).
- ⁹ S. P. Koenig, R. A. Doganov, H. Schmidt, A. H. Castro Neto, and B. zylmaz, *Appl. Phys. Lett.* **104**, 103106 (2014).
- ¹⁰ V. Tran, R. Soklaski, Y. Liang, and L. Yang, *Phys. Rev. B* **89**, 235319 (2014).
- ¹¹ Q. Wei and X. Peng, *Appl. Phys. Lett.* **104**, 251915 (2014).
- ¹² J.-W. Jiang and H. S. Park, *Nat. Commun.* **5**, 4727 (2014).
- ¹³ G. Qin, Q.-B. Yan, Z. Qin, S.-Y. Yue, H.-J. Cui, Q.-R. Zheng, and G. Su, *Scientific Reports* **4**, 6946 (2014).
- ¹⁴ H. Y. Lv, W. J. Lu, D. F. Shao, and Y. P. Sun, *Phys. Rev. B* **90**, 085433 (2014).
- ¹⁵ R. Fei, A. Faghaninia, R. Soklaski, J.-A. Yan, C. Lo, and L. Yang, *Nano Letters* **14**, 6393 (2014), pMID: 25254626, <http://dx.doi.org/10.1021/nl502865s>.
- ¹⁶ Z. Zhu and D. Tománek, *Phys. Rev. Lett.* **112**, 176802 (2014).
- ¹⁷ J. D. Wood, S. A. Wells, D. Jariwala, K.-S. Chen, E. Cho, V. K. Sangwan, X. Liu, L. J. Lauhon, T. J. Marks, and M. C. Hersam, *Nano Letters* **14**, 6964 (2014), pMID: 25380142, <http://dx.doi.org/10.1021/nl5032293>.
- ¹⁸ V. V. Kulish, O. I. Malyi, C. Persson, and P. Wu, *Phys. Chem. Chem. Phys.* **17**, 992 (2015).
- ¹⁹ G. A. Slack, *Phys. Rev.* **139**, A507 (1965).
- ²⁰ G. Kresse and J. Furthmüller, *Phys. Rev. B* **54**, 11169 (1996).
- ²¹ J. P. Perdew, K. Burke, and M. Ernzerhof, *Phys. Rev. Lett.* **77**, 3865 (1996).
- ²² H. J. Monkhorst and J. D. Pack, *Phys. Rev. B* **13**, 5188 (1976).
- ²³ L. Lindsay, D. A. Broido, and N. Mingo, *Phys. Rev. B* **82**, 115427 (2010).
- ²⁴ A. H. Castro Neto, F. Guinea, N. M. R. Peres, K. S. Novoselov, and A. K. Geim, *Rev. Mod. Phys.* **81**, 109 (2009).
- ²⁵ X. Zhang, H. Xie, M. Hu, H. Bao, S. Yue, G. Qin, and G. Su, *Phys. Rev. B* **89**, 054310 (2014).
- ²⁶ H. Xie, M. Hu, and H. Bao, *Appl. Phys. Lett.* **104**, 131906 (2014).
- ²⁷ R. Fei and L. Yang, *Nano Lett.* **14**, 2884 (2014).
- ²⁸ A. Togo, F. Oba, and I. Tanaka, *Phys. Rev. B* **78**, 134106 (2008).
- ²⁹ D. A. Broido, M. Malorny, G. Birner, N. Mingo, and D. A. Stewart, *Appl. Phys. Lett.* **91**, 231922 (2007).
- ³⁰ W. Li, L. Lindsay, D. A. Broido, D. A. Stewart, and N. Mingo, *Phys. Rev. B* **86**, 174307 (2012).
- ³¹ L. Lindsay, W. Li, J. Carrete, N. Mingo, D. A. Broido, and T. L. Reinecke, *Phys. Rev. B* **89**, 155426 (2014).
- ³² W. Li, J. Carrete, N. A. Katcho, and N. Mingo, *Comput. Phys. Commun.* **185**, 1747 (2014).
- ³³ J. Carrete, N. Mingo, and S. Curtarolo, *Appl. Phys. Lett.* **105**, 101907 (2014).
- ³⁴ D. Parker and D. J. Singh, *Phys. Rev. B* **82**, 035204 (2010).
- ³⁵ J. J. Pulikkotil, D. J. Singh, S. Auluck, M. Saravanan, D. K. Misra, A. Dhar, and R. C. Budhani, *Phys. Rev. B* **86**, 155204 (2012).
- ³⁶ T. Tritt, in *Thermal conductivity: theory, properties, and applications* (Kluwer Academic / Plenum Publishers, 2004) pp. 114–115.
- ³⁷ M. Hu, X. Zhang, and D. Poulikakos, *Phys. Rev. B* **87**, 195417 (2013).
- ³⁸ X. Gu and R. Yang, arXiv:1404.2874 (2014).